Engineering Structures 32 (2010) 2108–2121

Contents lists available at ScienceDirect

Engineering Structures

journal homepage: www.elsevier.com/locate/engstruct

Subassemblage tests and finite element analyses of sandwiched buckling-restrained braces

Chung-Che Chou [a,b,*], Sheng-Yang Chen [c]

[a] Department of Civil Engineering, National Taiwan University, Taipei, Taiwan
[b] National Center for Research on Earthquake Engineering, Taiwan
[c] Department of Civil Engineering, National Chiao Tung University, Hsinchu, Taiwan

ARTICLE INFO

Article history:
Received 29 December 2008
Received in revised form
6 March 2010
Accepted 9 March 2010
Available online 13 April 2010

Keywords:
Buckling-restrained brace
Chanel
Bolt
Cyclic test
Finite element analysis

ABSTRACT

This study presents the experimental and finite element analysis results of a proposed steel buckling-restrained brace (BRB). The proposed BRB has two components: (1) a steel core plate that carries all axial forces during tension and compression, and (2) two identical restraining members that sandwich the core plate with fully tensioned high-strength A490 bolts to prevent core buckling. Instead of using unbonded material, a small air gap is provided between the core plate and the restraining members to allow for lateral expansion of the core plate under compression. Since two restraining members can be disassembled easily by removing the bolts, a damaged steel core can be replaced after a large earthquake. Thus, manufacturing new restraining members is not required. Four BRB subassemblages were tested to investigate the inelastic deformation capabilities and verify the stability predictions for the braces. Test results indicate that three BRBs with sufficient flexural rigidity of the restraining member develop (1) stable hysteretic responses up to core axial strains of 2.1%–2.6%, (2) maximum compressive loads of 1724–1951 kN (1.4–1.6 times the actual yield load), and (3) a cumulative plastic ductility that is much higher than that specified in AISC seismic provisions (2005). One BRB, intentionally designed with inadequate flexural rigidity of the restraining member, experienced global buckling as predicted. Nonlinear finite element analysis was conducted for each BRB for a correlation study. The objective of the analysis was to conduct a parametric study for different BRBs to further verify the effects of restraining member size, number of bolts, core plate length and cross-sectional area on buckling load evaluation. The design procedure for the sandwiched BRB was provided based on test and finite element analysis results.

1. Introduction

Buckling-restrained braced frames (BRBFs) for seismic load resistance have been increasingly used in recent years [1–3]. A BRBF differs from a conventionally braced frame because a buckling-restrained brace (BRB) yields under both tension and compression without significant buckling. Numerous tests have been applied to different BRBs [4–12]. A typical BRB has a steel core encased in a restraining member consisting of a steel tube filled with concrete or mortar. A thin layer of an unbonded material is provided between the steel core and the surrounding concrete interface to eliminate force transfer and allow for lateral expansion of the steel core under compression [4–8,10–14]. Thus, the surrounding restraining member behaves as a continuous lateral bracing for the steel core. Such a BRB with an unbonded material as an interface to prevent adherence between the steel core and concrete has problems associated with quality control during manufacturing and flexibility at both ends of the BRB [10].

This study proposes a sandwiched BRB (Fig. 1) that eliminates the use of unbonded material in the manufacturing process and increases the number of design alternatives at both ends of the core plate for gusset connections. Two identical restraining members are formed by welding a steel channel to a flat plate (face plate) and then filled with concrete or mortar. Unlike conventional BRBs [4–10,12–14] that have a steel core inserted into a restraining member, sandwiching a core plate between a pair of restraining members using fully tensioned high-strength A490 bolts expedites the assembly process. Adding additional washers or a thin plate between the side plate and the face plate provides a small air gap between the core plate and face plate, allowing for expansion of the core plate under compression. There are two advantages to the proposed BRB over other conventional braces [4–10,12–14]. The first is the ability to disassemble the brace, which not only means that the core plate can be replaced independently of the restraining members, but also provides an opportunity for inspection of the

* Corresponding author at: Department of Civil Engineering, National Taiwan University, Taipei, Taiwan. Tel.: +886 2 3366 4349; fax: +886 2 2739 6752.
E-mail address: cechou@ntu.edu.tw (C.-C. Chou).

0141-0296/$ – see front matter © 2010 Elsevier Ltd. All rights reserved.
doi:10.1016/j.engstruct.2010.03.014

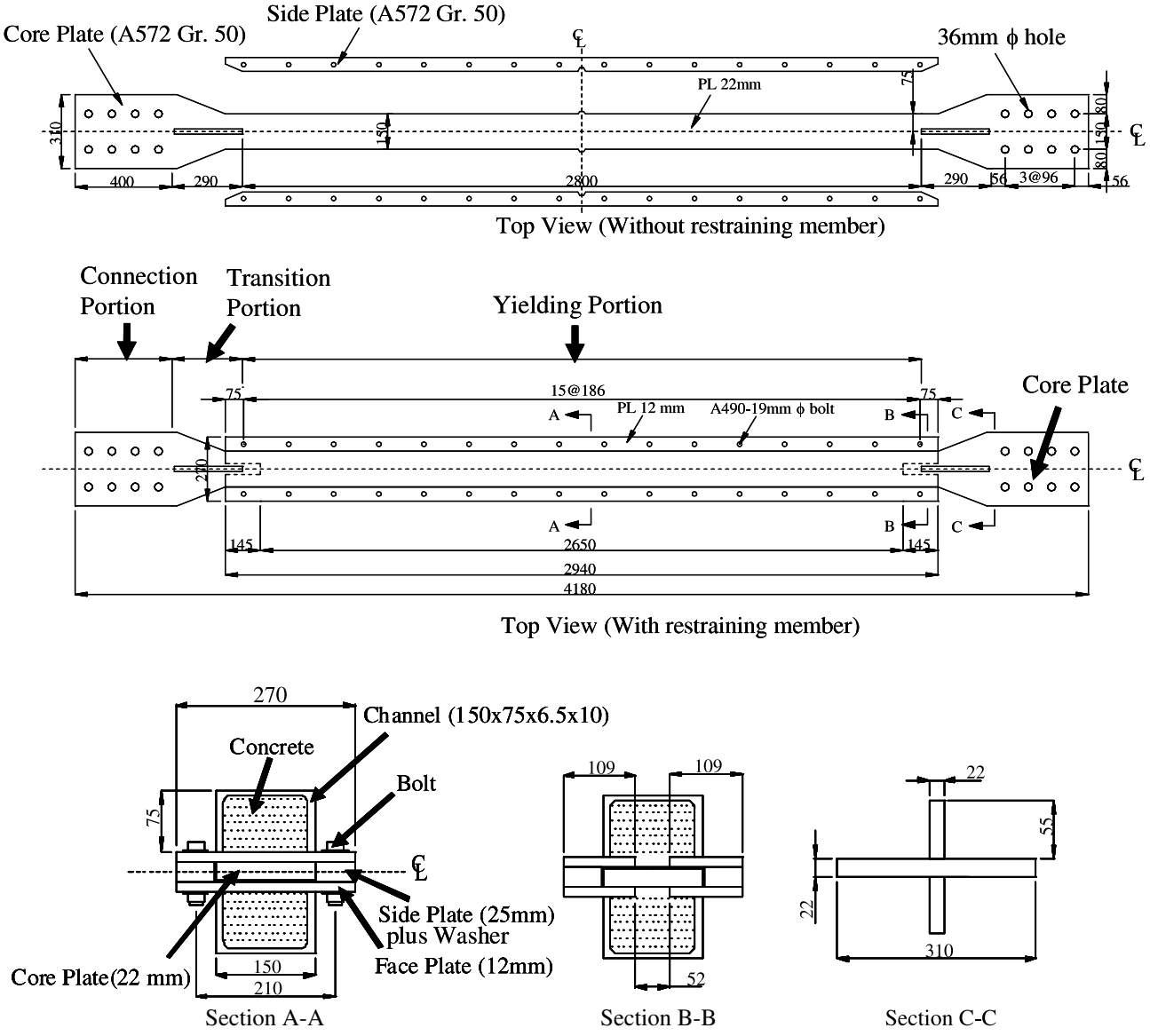

Fig. 1. Proposed buckling-restrained brace.

core. This is beneficial after a large earthquake or if used in an application such as a bridge superstructure [15] where high cycle fatigue is a concern. In case the core plate is damaged, replacing the core plate with recycle of restraining members of the proposed BRB is much cheaper than other conventional BRBs. The second is that in using conventional materials and providing a rational design basis, it opens up the opportunity for more widespread usage of BRBs, reducing the need for specialized design or fabrication. This, in the past, has limited the use of BRBFs unfairly over other poorer performing systems that require less performance verification. Furthermore, the core plate and restraining members can be delivered separately for on-site erection. A semi-circular tube may substitute for a rectangular channel to enhance architecturally appealing of the restraining member. A potential disadvantage of the proposed BRB is that it is slightly expensive with more parts (i.e. bolts) to assemble than some others in the first application.

Tests were conducted on four proposed BRBs designed with three performance parameters—moment of inertia of the restraining member and number and spacing of bolts. The test program investigated (1) the deformation capability of the proposed BRBs based on AISC loading protocol [16], (2) whether buckling load of the BRB could be estimated based on the proposed methodology, and (3) the effects of restraining member size and number of bolts on BRB cyclic behavior. Nonlinear finite element analysis was conducted for each BRB for correlation analysis. The objective of the analysis was (1) to conduct a parametric study of different BRBs to verify the effectiveness of the restraining member and number of bolts in preventing steel core buckling, and (2) to study the effects of BRB length and cross-sectional area on buckling load variation. This work presents the behavior of the sandwiched BRB experimentally and analytically, and provides a design procedure for this BRB [17,18].

2. Buckling-restrained brace design

Global stability of the BRB is estimated using the Euler theory of buckling. Fig. 2(a) shows the schematic of the proposed BRB in compression; the bending moment at the center of the restraining member is

$$M_{cent} = \frac{i+g+e}{1-\frac{P_{\max,g}}{P_e}} P_{\max,g} \tag{1}$$

where i ($= L/1000$) is the initial imperfection at the center of the BRB, g is the gap between the core plate and restraining

member, e is the eccentricity at the BRB end [9,11], P_e is the Euler buckling load of the restraining member, and $P_{\max,g}$ is the maximum compressive force in the BRB. By considering two deformed restraining members as a unit element under bending, the plastic moment capacity of this unit element, M_p^g, is

$$M_p^g = Z_{gf}F_{nyf} + Z_{gc}F_{nyc} \tag{2}$$

where Z_{gf} and Z_{gc} are the plastic section modulus of the face plates and channels about the BRB centerline axis, respectively; and F_{nyf} and F_{nyc} are the nominal yield strength of the face plate and channel, respectively. According to Chapter I of the 2005 AISC Specification for Structural Steel Buildings (AISC-LRFD) [19], concrete flexural strength inside the restraining member is not considered. Assuming that the limit state of the restraining member is reached when $M_{cent} = M_p^g$, the maximum compressive load is obtained by re-arranging Eq. (1) as follows:

$$P_{\max,g} = \frac{M_p^g}{i + g + e + \frac{M_p^g}{P_e}}. \tag{3}$$

When the restraining member has sufficient bending rigidity, the steel core buckles into a high mode (Fig. 2(b)). The buckling wavelength, L_w, is approximated by applying the Euler formula for a core segment L_w with a buckling coefficient of 0.5 [9]:

$$L_w = \sqrt{\frac{4\pi^2 E_t I_c}{P_y}} \tag{4}$$

where I_c is the moment of inertia about the weak-axis of the core plate, E_t is the tangent modulus of the core plate, assumed as 0.05 times the elastic modulus, and P_y is the core plate yield force. The contact force, f, which acts on the restraining member, is estimated based on the gap between the core plate and restraining member and a quarter of a wavelength:

$$f = P_{\max,l}\frac{g}{L_w/4}. \tag{5}$$

As the wavelength, L_w, is close to or larger than a bolt spacing L_b, the maximum bending moment in a restraining member is approximated by positioning a contact force f at the center of the bolt spacing, L_b; a pin-supported boundary condition is assumed at bolt locations. The maximum compressive load of the BRB is reached when the maximum bending moment in a restraining member ($= L_b f/4$) equals the plastic moment capacity, M_p^l, which is provided by a face plate and a channel. Therefore, the maximum compressive load based on this limit state of high-mode buckling is

$$P_{\max,l} = \frac{M_p^l L_w}{gL_b}. \tag{6}$$

If the wavelength, L_w, is smaller than the bolt spacing, the maximum bending moment in a restraining member is computed based on the number and magnitude of contact force within the bolt spacing.

Fully tensioned high-strength bolts provide the clamping force to eliminate separation between restraining members and a core plate. As global buckling of the BRB is prevented, high-mode buckling of the steel core (Fig. 2(b)) produces contact forces along the core plate length. The number of bolts, N_b, is determined based on bolt tensile capacity and total contact force in the BRB. Each contact force, adjusted based on the ratio of L_b/L_w, is assumed uniformly distributed across the face plate width (Fig. 2(c)):

$$f_a = f\frac{L_b}{L_w}. \tag{7}$$

Assuming a hinge-supported boundary condition at a bolt location, face plate thickness is determined based on adjusted contact force f_a and the von Mises yield criterion at the end of the fillet weld (point A in Fig. 2(c)).

3. Test program

3.1. Specimen

The test program consisted of cyclic tests of four BRB specimens. Fig. 1 shows the dimensions of Specimen 1. Specimens 2–4 were identical to Specimen 1, except for the size of restraining members and number of bolts. Table 1 summarizes member sizes and weights of each specimen. Core plate width, b_c, and thickness, t_c, were 150 mm and 22 mm, respectively, for all specimens. The moment of inertia of the restraining members, $I_{r,g}$, was calculated by considering the contribution of the face plate I_f, channel I_c and concrete I_{con}. Precisely, the channel contributed over 50% of the overall moment of inertia of restraining members. The moment of inertia of restraining members decreased for Specimens 1–4 to investigate its effects on BRB cyclic behavior. All bolts in the restraining member were A490 high-strength structural bolts 19 mm (3/4 in.) in diameter.

ASTM A36 steel with a nominal yield strength of 250 MPa was specified for the channel, and ASTM Gr. 50 steel was specified for the core, side, and face plates. The specified 28-day concrete strength was 35 MPa. Table 2 lists data obtained from tensile coupon tests of steel plates and compressive strength of concrete cylinders at day of test. Table 3 lists the core plate yield load, P_y, calculated by multiplying the cross-sectional area, $A_c (= b_c \times t_c)$, and yield stress, F_y, obtained from the material tensile coupon test (Table 2). One parameter investigated in this test program was the ratio of P_e/P_y, which was obtained by dividing the buckling load of restraining members P_e by core plate yield load P_y. The ratio of P_e/P_y was 6.4–1.4 for Specimens 1–4. For Specimen 4, which had a ratio of P_e/P_y less than 1.5, global buckling was expected before the core plate reached ultimate compressive capacity, P_u [3,4]:

$$P_u = \beta F_u A_c \tag{8}$$

where β is the compression strength adjustment factor, and a value of 1.3 [16] is used to estimate maximum compressive force. Tensile strength F_u is obtained from the material tensile coupon test (Table 2). The buckling load of Specimen 4 obtained from the test can be used to verify the accuracy of the global buckling load prediction based on Eq. (3). The value in parentheses under ultimate load P_u (Table 3) is the ratio of P_u/P_y, which is greater than the ratios of $P_{\max,g}/P_y$ and $P_{\max,l}/P_y$ for Specimen 4. The smallest value of $P_{\max,g}/P_y$ and $P_{\max,l}/P_y$ is the predicted buckling load ($= 1.2P_y$) for Specimen 4. Specimen 3 was designed with a different number of bolts to investigate the effects of number of bolts (or spacing) on the cyclic performance of the BRB. The tensile capacity-to-demand (CD) ratio of the bolt caused by contact force in the BRB was 1.5–7.4 in each test (Table 3). The ratio of $P_{\max,l}/P_y$ based on the limit state of high-mode buckling decreased as the ratio of L_b/L_w increased; the values of L_b/L_w were 0.3–2.1.

3.2. Test setup

Fig. 3(a) shows the test setup including one column pin-supported to the laboratory strong floor and attached to a 2000 kN hydraulic actuator. The BRB specimen was positioned at an inclination of $\theta = 50^\circ$ with both ends sandwiched by dual gusset plates. The weak axis of the steel core plate was within the loading plane such that out-of-plane buckling could be observed easily during tests. The relationship between core plate strain ε_c and column drift angle α was determined based on axial deformation δ in the specimen [10]:

$$\varepsilon_c = \frac{L_b\alpha}{2L_y}\sin 2\theta \tag{9}$$

where $L_b (= 4992$ mm) is the length between working points chosen at the intersection of the centerlines of the column, BRB and base, and L_y ($= 2800$ mm (Fig. 1)) is the yield length of the

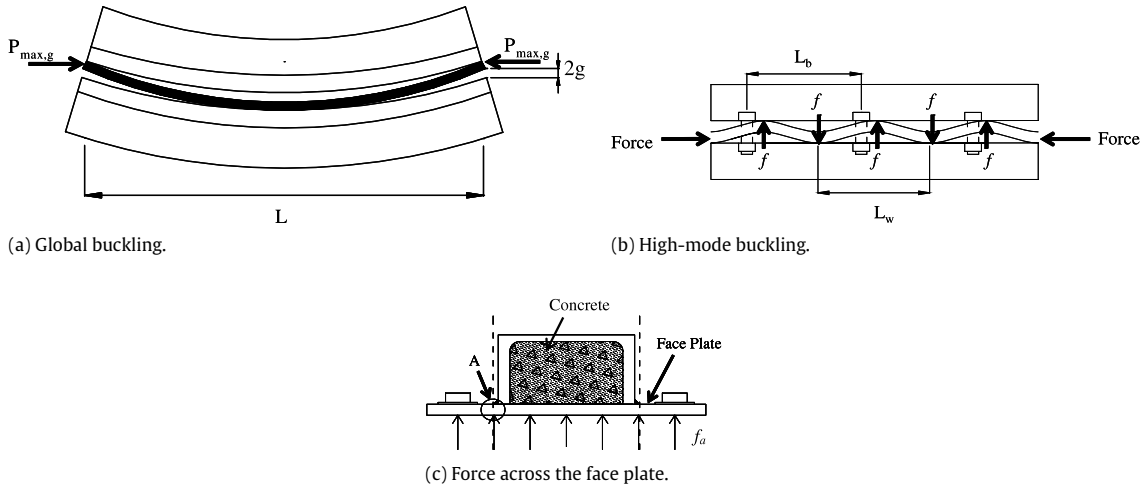

(a) Global buckling.

(b) High-mode buckling.

(c) Force across the face plate.

Fig. 2. BRB Behavior.

Table 1
Specimen dimension and weight.

(a) Dimension

Specimen no.	Core Plate			Channel and face plate (mm)	Restraining member			$I_{r,g}$ (mm^4)	Bolt (A490 3/4in)	
	b_c (mm)	t_c (mm)	L_y (mm)		$\frac{I_f}{I_{r,g}}$ (%)	$\frac{I_c}{I_{r,g}}$ (%)	$\frac{I_{con}}{I_{r,g}}$ (%)		No.	Spacing (mm) L_b
1	150	22	2800	150 × 75 × 6.5 × 10 270 × 12	3	68	29	44 432 996	32	186
2	150	22	2800	150 × 60 × 4.5 × 4.5 270 × 12	5	54	41	22 582 066	32	186
									80	72
3	150	22	2800	150 × 50 × 4.5 × 4.5 270 × 12	7	54	39	16 738 929	28	216
									16	432
4	150	22	2800	150 × 35 × 4.5 × 4.5 270 × 12	11	53	36	10 078 747	16	465

(b) Weight

Specimen no.	Steel core (kg)	Side plate (kg)	Face plate (kg)	Channel (kg)	Concrete (kg)	Total (kg)
1	140	95	150	109	144	638
2	140	95	150	54	120	559
3	140	95	150	50	96	529
4	140	95	150	44	72	501

Table 2
Material properties.

Specimen no.	Core plate		Channel		Face plate		Concrete strength (MPa)
	F_y[a] (MPa)	F_u[b] (MPa)	F_y (MPa)	F_u (MPa)	F_y (MPa)	F_u (MPa)	
1	367	525	274	425	441	565	57
2	372	528	285	434	411	558	57
3	364	530	285	434	411	558	58
4	375	506	279	438	389	515	48

[a] Yield strength.
[b] Ultimate strength.

core plate. The test specimen was subjected to prescribed loading in Section T6 of the AISC seismic provisions [16]. The loading protocol had two phases. First, each specimen was subjected to an increasing axial strain history (called standard loading), defined at levels corresponding to column drift angles of 0.38, 0.6, 1.2, 1.8 and 2.4%, where core plate maximum strain was 2.1%. Specimens 1–3 were subjected to additional tests, including large-deformation, low-cycle fatigue tests at a core plate strain of 1.6%. Specimen 3 was then tested twice with standard loading after removing some bolts from the BRB. Fig. 3(b) shows the locations of displacement transducers used to measure the displacement quantities of interest. The out-of-plane deformation along the BRB length was also recorded.

3.3. Test result

Fig. 4 shows the measured force in Specimens 1 and 2 versus total displacement measured across the yielding portion of the BRB (the displacements measured by displacement transducers L2 and L3 in Fig. 3(b) were added and divided by 2). A displacement calculated based on displacement transducers L4, L5, L6 and L7 was close to that computed based on transducers L2 and L3. Specimens

Table 3
Specimen strength.

Spe. no.	Core plate			Restraining member						Bolt number		
	P_y (kN)	P_u (kN)	L_w (mm)	P_e (kN)	$\frac{P_e}{P_y}$	M_p^g (kN m)	$\frac{P_{max,g}}{P_y}$	M_p^l (kN m)	$\frac{P_{max,l}}{P_y}$	N_b	CD[a]	$\frac{L_b}{L_w}$
1	1211	2252 (1.9)	210	7792	6.4	152.6	4.7	41.0	12.7	32	3.0	0.9
2	1228	2265 (1.8)	208	3949	3.2	95.6	2.5	20.8	6.3	32	3.0	0.9
									14	80	7.4	0.3
3	1201	2274 (1.9)	211	2943	2.5	84.6	2.0	17.6	4.8	28	2.6	1.0
									2.3	16	1.5	2.1
4	1238	2171 (1.8)	208	1758	1.4	74.3	1.2	13.5	1.3	16	1.5	2.2

[a] Bolt tensile capacity-demand ratio.

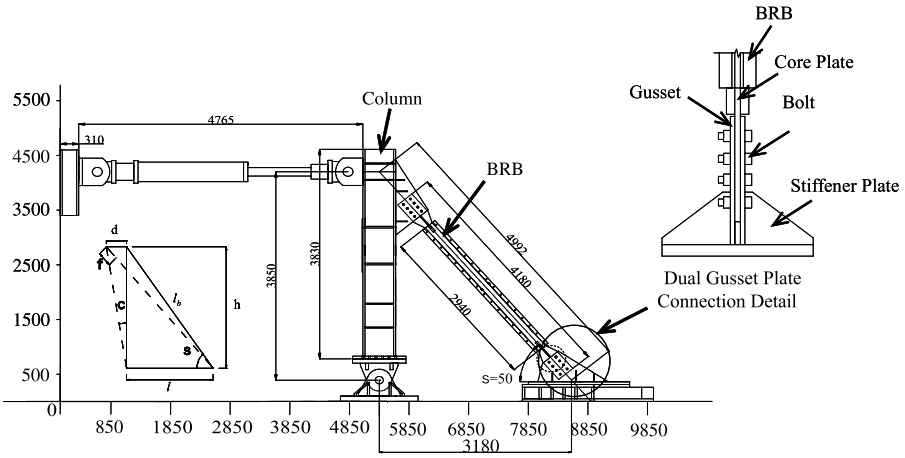

(a) Test setup (unit:mm).

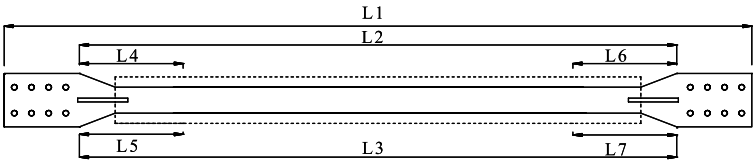

(b) Location of displacement transducer.

Fig. 3. Test setup and location of displacement transducer.

1 and 2 exhibited stable hysteretic responses up to a core strain of 2.1% during the standard loading test (Fig. 4(a) and (b)). No yielding or buckling of the restraining member was observed after the test (Fig. 5(a)); however, residual displacement was evident at both ends of the BRB (Fig. 5(b)). Fig. 4(c) and (d) show the force and displacement loops up to failure resulting from the low-cycle fatigue test. Specimens 1 and 2 exhibited stable hysteretic responses for the entire fatigue test consisting of 21 and 8 cycles, respectively. Specimen 2 had a few cycles because two additional standard loading histories were conducted up to a core strain of 1.3% in tension and 2.1% in compression. A measure to describe the plastic demand on a BRB is the cumulative plastic ductility, u_c, which is a normalized expression of the cumulative plastic deformation and is defined by

$$\mu_c = \sum_i \frac{\left|\Delta_{p_i}^+ - \Delta_{p_i}^-\right|}{\Delta_y} \tag{10}$$

where $\Delta_{p_i}^+$ and $\Delta_{p_i}^-$ are the maximum and minimum plastic displacements, respectively, during each cycle i into the inelastic range, and Δ_y is the axial displacement at first significant yield of the specimen [7,8]. Table 4 lists the cumulative plastic ductility for each test. Summation of the cumulative plastic ductility for all tests, $\Sigma\mu_c$, was 804 and 650 for Specimens 1 and 2, respectively, larger than the minimum required value of 200 by AISC seismic provisions [16]. These two specimens after all tests were disassembled by removing all bolts. A fracture was identified near the core plate center (Fig. 6(a) and (b)); the restraining members were undamaged.

Specimen 3 was first tested with 80 bolts connecting the core plate and restraining members. The specimen exhibited stable hysteretic behavior during the first standard and low-cycle fatigue tests (Fig. 7(a) and (b)). The cumulative plastic ductility after two complete cycles of the fatigue test was 256 (Table 4), already exceeding the AISC value. After removing 52 bolts, Specimen 3 was retested with a standard loading to a core axial strain of 2.1% (Fig. 7(c)); the restraining member was still undamaged. Twelve additional bolts were then removed such that the bolt spacing was 432 mm (Table 1). This specimen was again subjected to standard loading and exhibited stable hysteretic response up to a core strain of 2.6%. Weak-axis global buckling was observed during the third loading cycle at a core strain of 2.6% (Figs. 7(d) and 8(a)). The

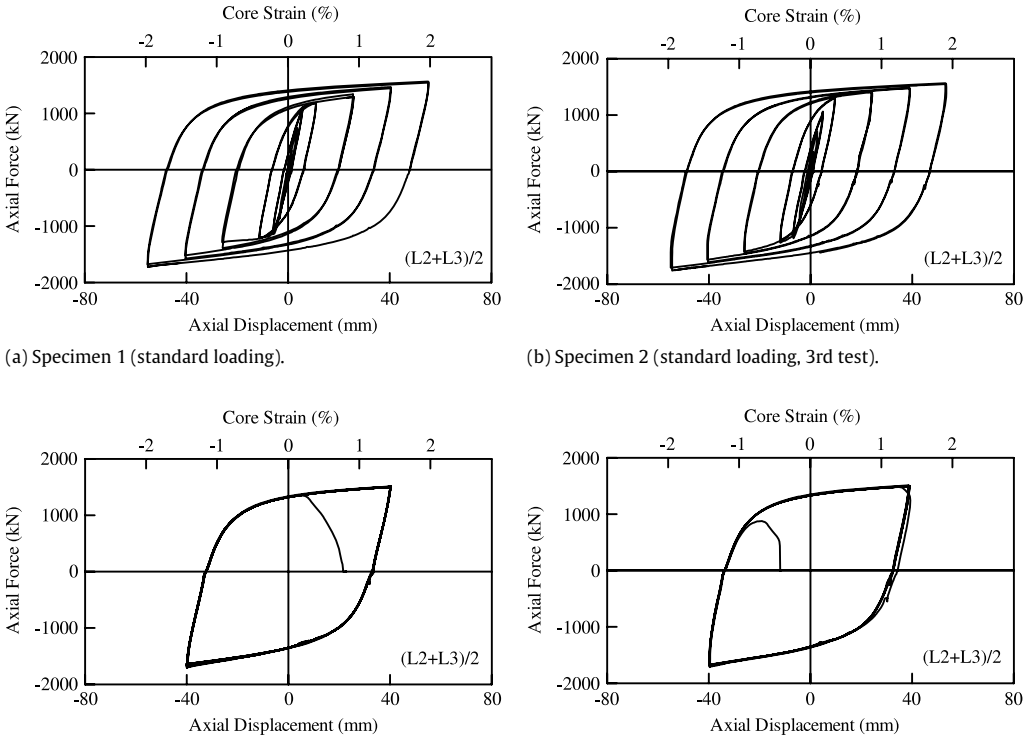

(a) Specimen 1 (standard loading).

(b) Specimen 2 (standard loading, 3rd test).

(c) Specimen 1 (fatigue loading, 21 cycles).

(d) Specimen 2 (fatigue loading, 8 cycles).

Fig. 4. Specimens 1 and 2 hysteretic responses.

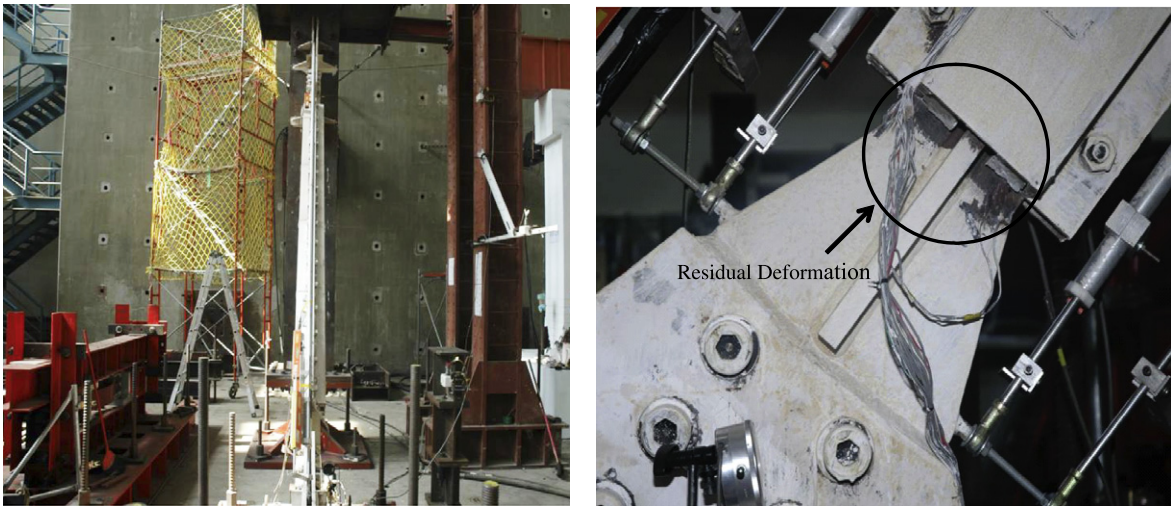

(a) Overall view.

(b) Residual deformation.

Fig. 5. Specimen 1 observed performance (after standard loading test).

steel channel bulged on the compression side of the restraining member (Fig. 8(b)). No slippage occurred between the core plate and restraining members. Additionally, no buckling of the dual gusset plate connections was noted; thus, the unbraced buckling length of the BRB was measured between the end of the top and bottom dual gusset plate connections. The cumulative plastic ductility after all tests was 767, close to that of Specimen 1.

Specimen 4 had $P_{max,g}/P_y$ and $P_{max,l}/P_y$ ratios that were less than P_u/P_y (Table 3), indicating that this specimen did not develop the ultimate load, as observed in Specimens 1–3. Instead, weak-axis global buckling was expected during the standard loading test to verify the prediction based on Eq. (3). This specimen showed stable hysteretic responses prior to global buckling at a core strain of 1.6% (Fig. 9(a)); maximum force in the BRB was 1494 kN in tension and 1660 kN in compression. The maximum compressive load divided by yield load P_y was 1.3, slightly larger than the predicted value of $P_{max,g}/P_y = 1.2$ (Table 3). Fig. 9(b) and (c) show the measured out-of-plane deformation for Specimens 3 and 4 under compression. The out-of-plane deformation was small prior to global buckling and increased suddenly when global buckling occurred. Note that Specimens 3 and 4 buckled in opposite directions. Fig. 6(c) and (d) show global buckling of core plates after disassembling Specimens 3 and 4; core plates had no cracks. The ratio of maximum compressive force to maximum tensile force was 1.1–1.15 for all specimens, less than 1.3 specified in AISC seismic provisions [16].

(a) Specimen 1.

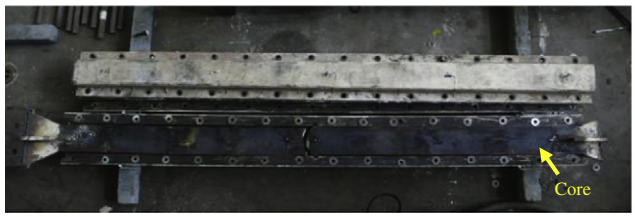

(b) Specimen 2.

(c) Specimen 3.

(d) Specimen 4.

Fig. 6. Failure modes of all specimens after tests.

Table 4
Specimen test results.

Specimen no.	Test no.	Test phase	α_{max} [a] (%)	ε_{max} [b] (%)	μ_{max} [c]	μ_c	$\Sigma\mu_c$	Final failure mode	
								Core	Restraining member
1	First	Standard	2.4	2.1	11.4	196	804	Tensile fracture	No
		Fatigue	1.8		8.5	608			
2	First	Standard	2.4	2.1	11.4	106	650	Tensile fracture	No
	Second	Standard	2.4		11.4	106			
	Third	Standard	2.4		11.4	196			
		Fatigue	1.8		8.5	242			
3	First	Standard	2.4	2.6	11.4	196	767	Global buckling	Global buckling
		Fatigue	1.8		8.5	60			
	Second	Standard	2.4		11.4	196			
	Third	Standard	3.0		14.2	315			
4	First	Standard	1.8	1.6	8.5	120	120	Global buckling	Global Buckling

[a] Maximum column drift angle.
[b] Maximum core axial strain.
[c] Maximum ductility.

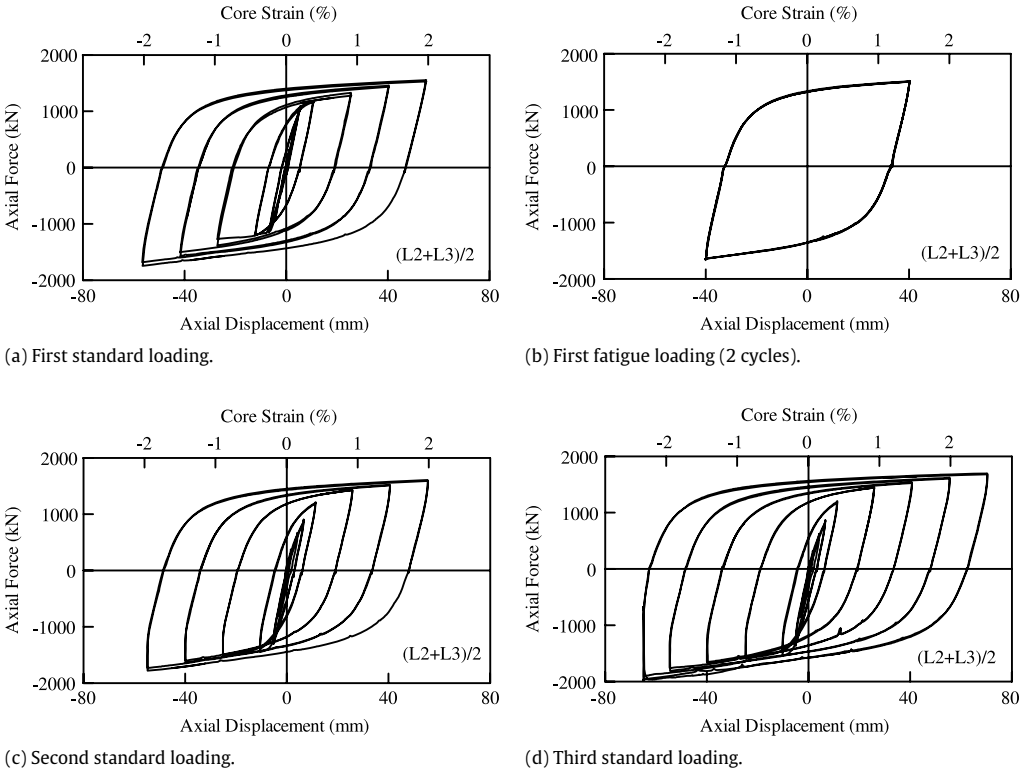

(a) First standard loading.

(b) First fatigue loading (2 cycles).

(c) Second standard loading.

(d) Third standard loading.

Fig. 7. Specimen 3 hysteretic responses.

(a) Global buckling of BRB.

(b) Bulging of steel channel.

Fig. 8. Specimen 3 observed performance (axial strain of 2.6% during third standard loading test).

4. Finite element analysis

4.1. Finite element models for test specimens

To provide a better understanding of the compressive behavior and buckling load of BRBs, an analytical study using the finite element computer program ABAQUS [20] was conducted for 22 BRB models. Specimens 1–4, called Models 1–4, respectively, were first analyzed for a correlation study. Material nonlinearity with the von Mises yielding criterion was considered in the steel core and restraining members. Yield stress obtained from the coupon test (Table 2) was adopted independently for each specimen. The elastic modulus of steel was 203 GPa. To consider the cyclic effects of BRBs in the tests, the combined isotropic and kinematic hardening model in the computer program ABAQUS was used. The corresponding parameters, which were determined from the cyclic responses of steel coupons, can be found from the prior work [21,22]. Concrete infill was modeled with an elastic property. The steel core, restraining member, concrete infill, and bolts were modeled using eight-node solid elements, C3D8R. Since no slippage existed between the core plate and restraining members in all specimens, rigid beams were used to simulate all bolted connections. The side plates had holes at bolted locations for passing through these rigid beams. An interaction between the steel core and a restraining member was modeled with a hard contact behavior, allowing separation of the interface in tension

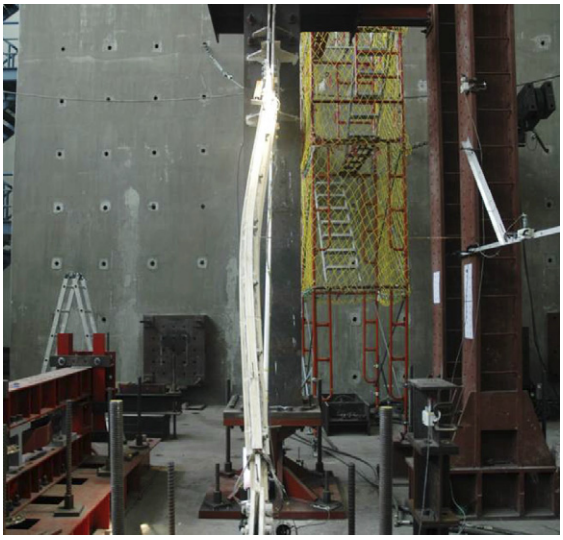

(a) Specimen 4 global buckling (axial strain of 1.6%, 1st standard loading test).

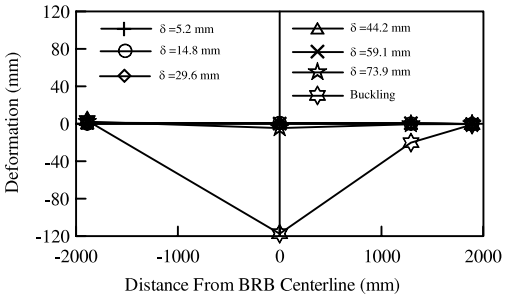

(b) Out-of-plane deformation (specimen 3).

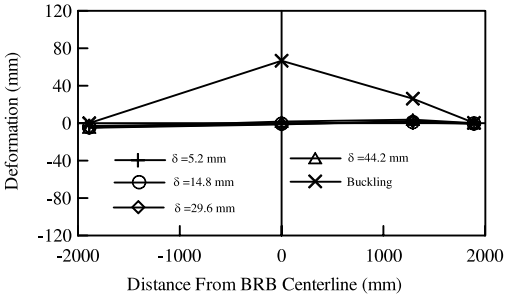

(c) Out-of-plane deformation (specimen 4).

Fig. 9. Out-of-plane deformation of the BRB.

and no penetration of that in compression [23]. A frictional coefficient of 0.1 was adopted to simulate greasy steel interfaces.

Fig. 10(a) shows the different parts of Model 1 prior to assembly and a cross-sectional view of Model 1 after assembly. Fig. 10(b) shows the first buckling mode of the core plate. An initial imperfection shape of the core plate (1/3000 of the core length) was adopted by scaling the first buckling mode. An axial displacement was then applied to the end of the core plate to obtain monotonic behavior. Fig. 11 shows core plate deformation in Models 1 and 4 under increasing axial displacement. The number of waves, n, increases as axial displacement, δ, increases; a total of 12 waves are observed when models reach yield ($\delta = 5.2$ mm). Model 1 had no global buckling at an axial displacement of $\delta = 59.1$ mm (equal to 2.2% of core axial strain) and no strength degradation in the relationship between axial force and axial deformation (Fig. 12(a)). Model 4 buckled globally with 12 waves at $\delta = 39.3$ mm. The maximum compressive load of Model 4 was 1697 kN, close to 1660 kN obtained during the cyclic test (Fig. 12(b)). Generally, the finite element models reasonably predicted initial elastic stiffness and post-yield strength of BRBs tested.

4.2. Parametric study

The objective of the parametric study was to investigate the effects of core plate size, restraining member size, and number of bolts on BRB buckling load. The parameters were length and cross-sectional area of the core plate, bolt spacing, and moment of inertia of the restraining member. In total, 18 BRBs were modeled. Model details are listed in Table 5. Models 5–13 represented BRBs with three yield lengths (L_y) and three cross-sectional areas ($A_c = b_c \times t_c$); restraining members were designed with a bolt CD ratio of 1.5, L_b/L_w ratios of 1.3–2.1 (Table 6), and P_e/P_y ratios of 2.0–2.5 (Table 6). Models 14–22 had either ratios of $P_{\max,g}/P_y$ or $P_{\max,l}/P_y$ close to 1.0 (Table 6) to obtain buckling load for verification.

Fig. 13(a) shows the relationship between axial compressive force and axial compressive strain for Models 5–7 and 14–16, which had an $A_c = 1500$ mm^2. No strength degradation was noted at a core compressive strain of 3.2% for Models 5–7, which had ratios of P_e/P_y of about 2.5, L_b/L_w of about 2, and a CD ratio of 1.5. However, Models 14 and 15, even with ratios of P_e/P_y of about 2.5, experienced local buckling and strength degradation due to low CD values (Table 5) and large ratios of L_b/L_w (Table 6). Fig. 14 (a) and (b) show high-mode buckling of the core plate at peak loading, resulting in local buckling of restraining members between two bolts. Model 16 experienced global buckling due to a low P_e/P_y ratio of 1.25.

Fig. 13(b) shows the relationship between axial compressive force and axial compressive strain for Models 3, 4, 8, 9, and 17–19, which had an $A_c = 3300$ mm^2. No strength degradation was noted at a core compressive strain of 3.2% for Models 3, 8, and 9, which had ratios of P_e/P_y of about 2.5, L_b/L_w of 1.3–2.1, and a CD ratio of 1.5. Model 17 was identical to Model 3, except that the bolt spacing for Model 17 was larger than that for Model 3; the ratio of L_b/L_w for Model 17 was 2.65. Model 17 showed local buckling of the restraining member at a low core compressive strain but the strength did not decrease until at a core compressive strain of 1.8%. Model 4, which simulated Specimen 4, experienced global buckling as seen in Fig. 14(c). Model 18 was identical to Model 4, except that bolt spacing for Model 18 was 1.5 times that for Model 4 and the

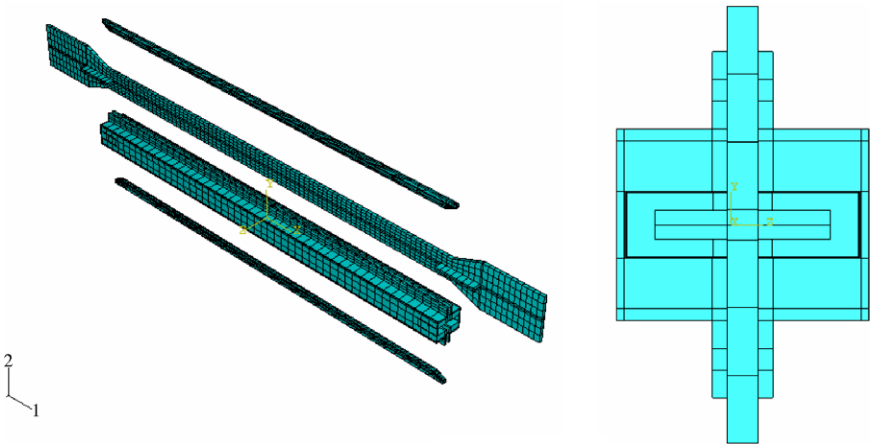

(a) Model.

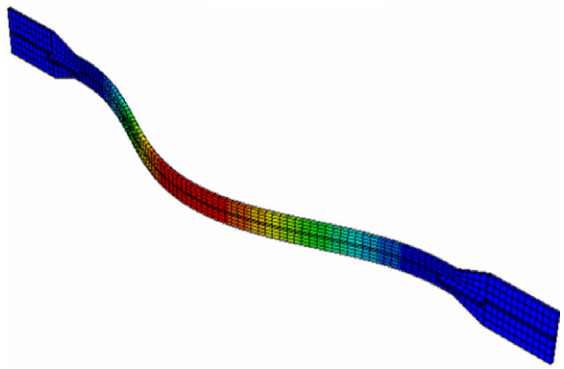

(b) First buckling mode of steel core plate.

Fig. 10. Specimen 1 finite element model.

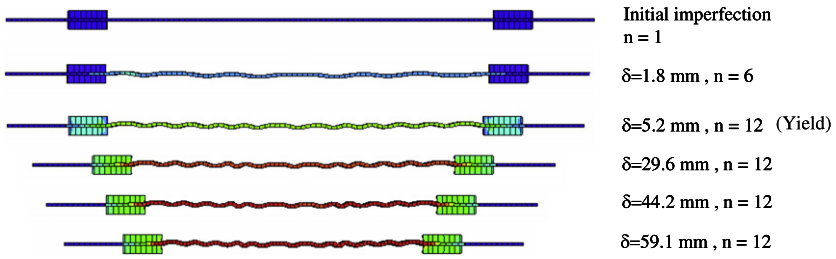

(a) Model 1 (specimen 1).

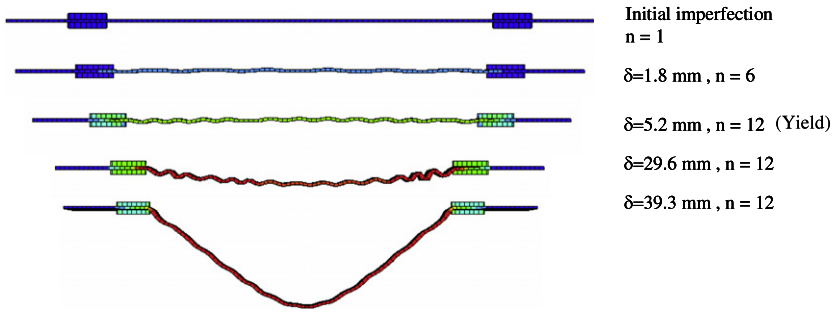

(b) Model 4 (specimen 4).

Fig. 11. Core plate buckling in increasing axial displacement.

bolt CD ratios were 1 and 1.5 for Models 18 and 4, respectively. Local buckling of the restraining member occurred in Model 18 at a core compressive strain of 0.18%, much lower than that when Model 4 buckled. Model 19 was identical to Model 8, except that the ratio of P_e/P_y for Model 19 was half that for Model 8. Global buckling occurred in Model 19 at a core compressive strain of 1.0%.

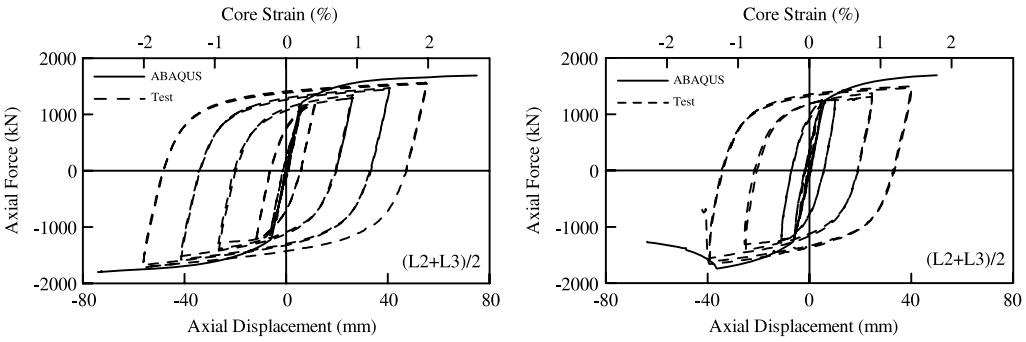

(a) Mode1 (specimen 1). (b) Model 4 (specimen 4).

Fig. 12. Comparison between test and finite element analysis results.

Table 5
Model details.

Model		Core Plate				Restraining member				Bolt			
No.	Name	b_c (mm)	t_c (mm)	Yield stress (MPa)	L_y (mm)	Channel (mm)	Face plate (mm)	Length (mm)	$I_{r,g}$ (mm^4)	Bolt size (mm)	N_b	L_b (mm)	CD
5	A15L28P24S	100	15	375	2800	100 × 46 × 4.5 × 4.5	200 × 10	2940	7767168	16	22	280	1.5
6	A15L48P25S	100	15	375	4800	100 × 76 × 4.5 × 4.5	200 × 10	4940	20138857	16	36	282	1.5
7	A15L96P25S	100	15	375	9600	100 × 134 × 4.5 × 4.5	200 × 10	9740	72688354	16	74	267	1.5
3	A33L28P24S	150	22	364	2800	150 × 50 × 4.5 × 4.5	270 × 12	2940	16738929	19	16	432	1.5
8	A33L48P24S	150	22	375	4800	C 150 × 75 × 6.5 × 10	270 × 12	4940	43695988	16	36	284	1.5
9	A33L96P25S	150	22	375	9600	150 × 156 × 4.5 × 4.5	270 × 12	9740	159846725	16	72	274	1.5
10	A64L28P24S	200	32	375	2800	200 × 56 × 4.5 × 4.5	320 × 14	2940	33266295	19	14	455	1.5
11	A64L48P23S	200	32	375	4800	C 200 × 80 × 7.5 × 11	320 × 14	4940	80615534	19	24	438	1.5
12	A64L96P25S	200	32	375	9600	200 × 178 × 4.5 × 4.5	320 × 14	9740	309930822	19	48	418	1.5
13	A64L48P20S	200	32	375	4800	200 × 88 × 4.5 × 4.5	320 × 14	4940	69940478	19	24	438	1.5
14	A15L28P24LB	100	15	375	2800	100 × 46 × 4.5 × 4.5	200 × 10	2940	7767168	16	14	467	1.0
15	A15L48P25GB	100	15	375	4800	100 × 76 × 4.5 × 4.5	200 × 10	4940	20138857	16	16	686	0.7
16	A15L96P13GB	100	15	375	9600	100 × 100 × 4.5 × 4.5	200 × 10	9740	36613236	16	74	267	1.5
17	A33L28P24LB	150	22	364	2800	150 × 50 × 4.5 × 4.5	270 × 12	2940	16738929	19	12	560	1.2
4	A33L28P14GB	150	22	375	2800	150 × 35 × 4.5 × 4.5	270 × 12	2940	10078747	19	16	465	1.5
18	A33L28P14LB	150	22	375	2800	150 × 35 × 4.5 × 4.5	270 × 12	2940	10078747	19	10	700	1.0
19	A33L48P12GB	150	22	375	4800	150 × 60 × 4.5 × 4.5	270 × 12	4940	22016167	16	36	284	1.5
20	A64L28P24LB	200	32	375	2800	200 × 56 × 4.5 × 4.5	320 × 14	2940	33266295	19	10	700	1.1
21	A64L48P13GB	200	32	375	4800	200 × 68 × 4.5 × 4.5	320 × 14	4940	44694868	19	24	438	1.5
22	A64L96P14GB	200	32	375	9600	200 × 140 × 4.5 × 4.5	320 × 14	9740	179652939	19	48	418	1.5

Table 6
Design parameters.

Model		Design parameters								ABAQUS	
No.	Name	P_y (kN)	P_u (kN)	L_w (mm)	$\frac{L_b}{L_w}$	P_e (kN)	$\frac{P_e}{P_y}$	$\frac{P_{\max\times,g}}{P_y}$	$\frac{P_{\max\times,l}}{P_y}$	Result	$\frac{P_{\max\times}}{P_y}$
5	A15L28P24S	563	987	142	1.97	1362	2.42	2.0	3.2	S[a]	1.42
6	A15L48P25S	563	987	142	1.99	1394	2.48	2.1	5.7	S	1.39
7	A15L96P25S	563	987	142	1.85	1405	2.50	2.1	13.8	S	1.38
3	A33L28P24S	1201	2274	211	2.05	2943	2.45	2.0	2.3	S	1.48
8	A33L48P24S	1238	2171	208	1.37	3025	2.44	2.1	8.1	S	1.47
9	A33L96P25S	1238	2171	208	1.32	3090	2.50	2.0	11.5	S	1.45
10	A64L28P24S	2400	4210	302	1.51	5834	2.43	1.9	2.3	S	1.50
11	A64L48P23S	2400	4210	302	1.45	5580	2.33	1.9	5.9	S	1.48
12	A64L96P25S	2400	4210	302	1.38	5999	2.50	1.9	9.2	S	1.47
13	A64L48P20S	2400	4210	302	1.45	4841	2.01	1.6	3.8	S	1.47
14	A15L28P24LB	563	987	142	3.3	1362	2.42	2.0	1.2	LB[c]	1.32
15	A15L48P25LB	563	987	142	4.83	1394	2.48	2.1	1.0	LB	1.19
16	A15L96P13GB	563	987	142	1.85	708	1.25	1.1	7.55	GB[b]	1.20
17	A33L28P24LB	1201	2274	211	2.65	2943	2.45	2.0	1.2	LB	1.13
4	A33L28P14GB	1238	2171	208	2.24	1758	1.42	1.2	1.3	GB	1.36
18	A33L28P14LB	1238	2171	208	3.37	1758	1.42	1.2	0.6	LB	0.58
19	A33L48P12GB	1238	2171	208	1.37	1357	1.23	1.1	3.7	GB	1.32
20	A64L28P24LB	2400	4210	302	2.3	5834	2.43	1.9	1.2	LB	0.97
21	A64L48P13GB	2400	4210	302	1.45	3244	1.29	1.1	3.0	GB	1.31
22	A64L96P14GB	2400	4210	302	1.38	3473	1.44	1.2	6.7	GB	1.31

[a] Successful (no buckling).
[b] Global buckling.
[c] Local buckling.

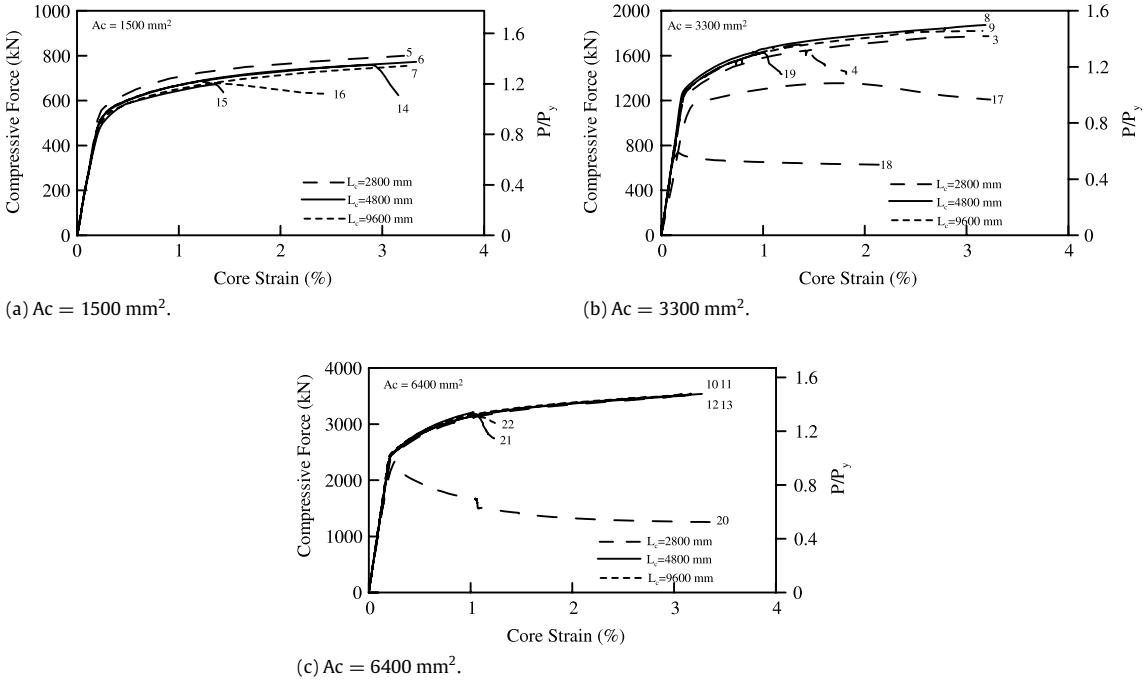

(a) Ac = 1500 mm².

(b) Ac = 3300 mm².

(c) Ac = 6400 mm².

Fig. 13. Axial force versus strain relationships.

Fig. 13(c) shows the relationship between axial compressive force and axial compressive strain for Models 10–13 and 20–22, which had an $A_c = 6400$ mm^2. Models 10–13, which had ratios of P_e/P_y of 2.0–2.5, L_b/L_w and bolt CD ratios of about 1.5, showed no buckling at a core compressive strain of 3.2%. Model 20 was identical to Model 10, except that the L_b/L_w and bolt CD ratios for Model 20 were 2.3 and 1.1, respectively. Local buckling was observed in Model 20 at a core compressive strain of 0.26%. Models 21 and 22 were identical to Models 11 and 12, respectively, except that Models 21 and 22 had low P_e/P_y ratios (Table 6). As expected, Models 21 and 22 experienced global buckling (Fig. 14(d)) at a low core compressive strain.

Fig. 15(a) shows the relationship between a ratio of maximum compressive load to yield load (P_{max}/P_y) and a ratio of L_b/L_w. For models with P_e/P_y ratios larger than 2 and L_b/L_wratios less than 2, the P_{max}/P_y ratios are close to 1.4–1.5 at a core compressive strain of 3.2% without buckling. The P_{max}/P_y ratios are 1.0–1.4 due to local buckling of the restraining member in models with P_e/P_y and L_b/L_wratios larger than 2. The P_{max}/P_y ratio in Model 18 is extremely low with $P_e/P_y = 1.4$ and $L_b/L_w = 3.4$. Fig. 15(b) shows the relationship between P_{max}/P_y and P_e/P_y ratios for all models with an L_b/L_w ratio less than 2, such that local buckling of the restraining member is excluded. Note that the ratio of P_{max}/P_y increases as P_e/P_y increases and reaches about 1.4–1.5 when the P_e/P_y ratio exceeds 2. Fig. 15(c) shows the relationship between P_{max}/P_y and $I_{r,g}/(I_{r,g})_{min}$ for models with similar P_e/P_y ratios (>2) and different core plate yield lengths and thicknesses. For a specified core plate yield length, the ratio of $I_{r,g}/(I_{r,g})_{min}$ is computed by dividing the moment of inertia of the restraining member $I_{r,g}$ by that ($(I_{r,g})_{min}$) of a model with the thinnest core plate. The P_{max}/P_y ratio increases as core plate thickness increases. For core plates with the same thickness, the P_{max}/P_y ratio increases as core plate length decreases. Fig. 15(d) shows a comparison between maximum compressive load obtained by finite element analysis (P_{max}/P_y) and buckling load prediction ($(P_{max}/P_y)_p$), which is the minimum value of $P_{max,g}/P_y$ and $P_{max,l}/P_y$ in models (Table 6). The prediction based on Eq. (3) or (6) is reasonably accurate, conservatively estimating maximum compressive load for most models.

5. Recommended design procedure

A parametric study shows the effects of restraining member size, number of bolts, core plate length and cross-sectional area on buckling load variation, indicating that for models with a P_e/P_y ratio larger than 2, L_b/L_w ratio less than 2 and bolt CD ratio of 1.5, maximum compressive load of the BRB reaches about 1.4–1.5P_y without buckling. The restraining member and number of bolts should be designed based on ratios of $P_e/P_y \geq 2.5$, $L_b/L_w \leq 2.0$, and bolt CD ratio ≥ 1.5, such that the compressive load $P_{max,g}$ or $P_{max,l}$ exceeds P_u to exclude buckling. A stringent requirement for a P_e/P_y ratio is recommended due to the smallest value of P_e/P_y among Specimens 1–3 (Table 3). The following steps for designing the proposed BRB are recommended:

1. Determine the cross-sectional area of the core plate using Eq. (8). Note that the ratio of maximum compressive force to maximum tensile force β can, based on test results, be 1.15 instead of 1.3 as recommended in AISC seismic provisions [16].

2. Compute the moment of inertia of the restraining member based on yield load of core plate P_y and $P_e/P_y \geq 2.5$ to determine the preliminary size of the restraining member. It is recommended that the channel and core plate widths be similar and the channel provide more than half the total moment of inertia of the restraining member based on design characteristics of test specimens (Table 1(a)).

3. Compute plastic moment capacity of the restraining member M_p^g (Eq. (2)) and maximum compressive load based on the limit state of global buckling $P_{max,g}$ (Eq. (3)). If $P_{max,g}$ is less than P_u, determine the other restraining member dimensions by returning to Step 2.

4. Calculate buckling wavelength L_w (Eq. (4)) and maximum compressive load based on the limit state of high-mode buckling $P_{max,l}$ (Eq. (6)). If $P_{max,l}$ is less than P_u, determine the other restraining member dimensions by returning to Step 2.

5. Estimate contact force f (Eq. (5)). The number of bolts, N_b, is determined by bolt tensile capacity and total contact force in the BRB with a bolt CD ratio of 1.5. If bolt spacing L_b does not satisfy $L_b/L_w \leq 2.0$, the number of bolts should be increased.

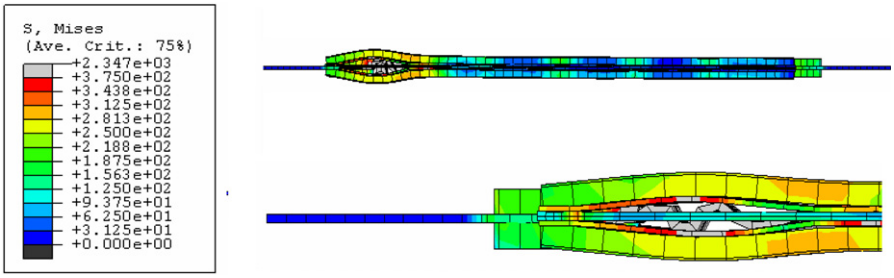

(a) Model 14.

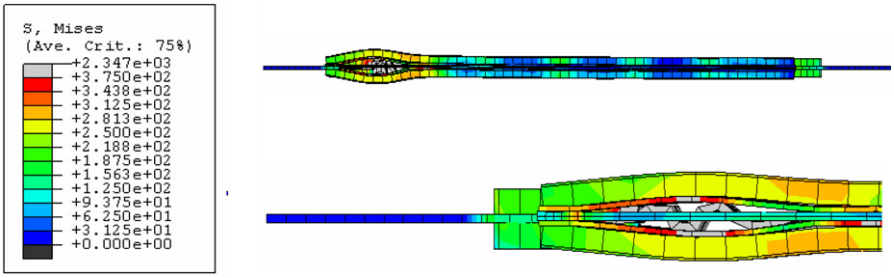

(b) Model 15.

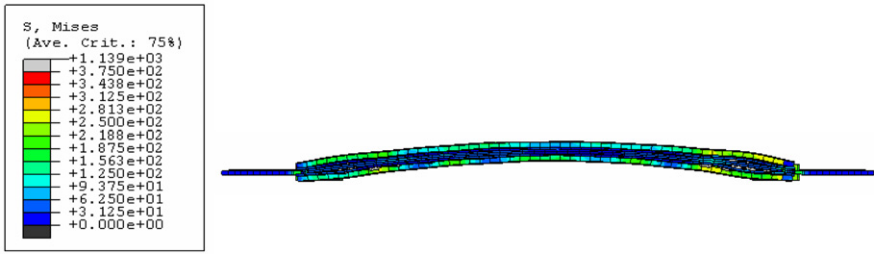

(c) Model 4.

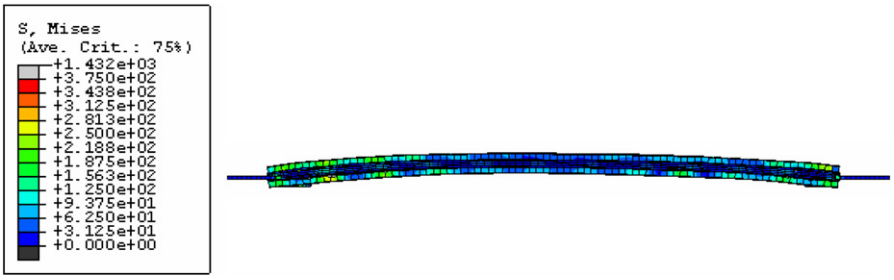

(d) Model 21.

Fig. 14. Global and local buckling of finite element models.

6. Conclusions

A BRB was developed by sandwiching a core plate between two restraining members, which were made of a flat plate, channel and in-filled concrete, with fully tensioned high-strength A490 bolts. Specimens 1–3, designed with ratios of $P_e/P_y \geq 2.5$ and $L_b/L_w \leq 2.1$ and a bolt CD ratio ≥ 1.5, had stable hysteretic responses and developed maximum compressive loads of 1724–1951 kN (1.4–1.6 times actual yield load P_y) at compressive strains of 2.1%–2.6%. The cumulative plastic ductility was 650–804, significantly larger than the minimum required cumulative plastic ductility of 200 specified in AISC seismic provisions [16]. Specimen 4 was designed with a P_e/P_y ratio of 1.4 to verify the accuracy of buckling load prediction (Eq. (3)). Specimen 4 also exhibited stable hysteretic responses prior to global buckling at a core compressive strain of 1.6%. Finite element analysis was conducted for correlation and parametric studies to examine the effects of flexural rigidity of the restraining member, bolt spacing, core plate length and cross-sectional area on BRB buckling load. This study supports recommended design criteria for the proposed BRB and obtains the following conclusions.

1. A small gap substituting unbonded material between the core plate and restraining members does not affect the cyclic behavior of the proposed BRB. The ratio of maximum compressive force to maximum tensile force is 1.1–1.15, less than the ratio of 1.3 in AISC seismic provisions [16].

2. Specimens 1 and 2 exhibited core plate fractures during low-cycle fatigue tests. The BRB was disassembled by removing all bolts. One crack propagated through the core width near the center of the BRB. The restraining members in Specimens 1 and 2 did not yield or buckle after all tests. Specimen 3 tested three times with different number of bolts showed similar hysteretic responses up

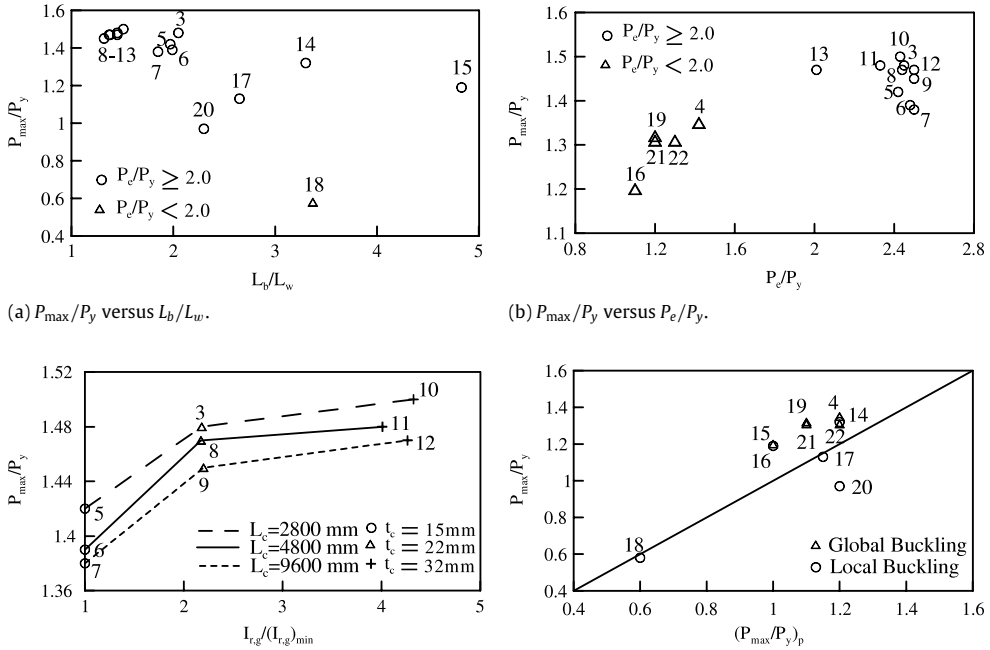

(a) P_{max}/P_y versus L_b/L_w.

(b) P_{max}/P_y versus P_e/P_y.

(c) p_{max}/P_y versus $I_{r,g}/(I_{r,g})min$.

(d) Finite element analysis versus prediction.

Fig. 15. Comparison between different parameters.

to a core compressive strain of 2.6%. The global buckling load of Specimen 4 was 1.3 P_y, slightly larger than the predicted value of $P_{max,g} = 1.2P_y$ using Eq. (3) and close to the buckling load based on finite element analysis.

3. A parametric study, conducted on 18 BRBs, demonstrated that the predicted maximum load based on the limit state of either global or local buckling (Eq. (3) or (6)) was reasonably accurate, conservatively estimating maximum compressive loads for most models. For core plates with the same thickness, theP_{max}/P_y ratio increases as core plate length decreases. For core plates with the same length, the P_{max}/P_y ratio increases as core plate thickness increases.

4. A parametric study showed that if the restraining member of the BRB was designed with $P_e/P_y \geq 2.0$, $L_b/L_w \leq 2.0$, and a CD ratio $\geq$ 1.5 (Models 5–13), the BRB reached a maximum compressive load of about 1.4–1.5P_y (Table 6) without buckling. A stringent requirement for a ratio of $P_e/P_y \geq 2.5$ was proposed due to the smallest value of P_e/P_y among Specimens 1–3 (Table 3).

Acknowledgements

The financial support provided by the National Center for Research on Earthquake Engineering (NCREE), Taiwan is appreciated. The authors would like to thank Prof. K. C. Tsai for providing advice in this research program.

References

[1] Sabelli R, Mahin SA, Chang C. Seismic demands on steel braced-frame buildings with buckling-restrained braces. Eng Struct 2003;25:655–66.
[2] Kiggins S, Uang CM. Reducing residual drift of buckling-restrained braced frames as a dual system. Eng Struct 2006;28:1525–32.
[3] Uang CM, Nakashima M. Steel buckling-restrained braced frames. In: Bozorgnia Y, Bertero VV, editors. Earthquake engineering from engineering seismology to performance-based engineering. Boca Raton, FL: CRC Press LLC; 2003. p. 16-1–16-37. [Chapter 16].
[4] Watanabe A, Hitomi Y, Yaeki E, Wada A, Fujimoto M. Properties of braces encased in buckling-restraining concrete and steel tube. In: Proceedings of 9th world conference on earthquake engineering. 1988. p. 719–24.
[5] Wada A, Saeki E, Takeuchi T, Watanabe A. Development of unbonded brace. Nippon Steel Corporation Building Construction and Urban Development Division, Tokyo, Japan, 1998. p. 1–16.
[6] Clark P, Aiken I, Kasai K, Ko E, Kimura I. Design procedures for buildings incorporating hysteretic damping devices. In: Proceedings of 69th annual convention. SEAOC. 1999.
[7] Merritt S, Uang CM, Benzoni G. Subassemblage testing of CoreBrace buckling-restrained braces. Report No. TR-2003/01. University of California, San Diego; 2003.
[8] Merritt S, Uang CM, Benzoni G. Subassemblage testing of Star Seismic buckling-restrained braces. Report No. TR-2003/04. University of California, San Diego; 2003.
[9] Koetaka Y, Byakuno Y, Inoue K. Experimental verification of design criteria of knee brace damper. in: 8th Taiwan–Korea–Japan Joint seminar on earthquake engineering for building structures. 2006. p. 69–79.
[10] Iwata M, Murai M. Buckling-restrained brace using steel mortar planks: performance evaluation as a hysteretic damper. Earthq Eng Struct Dyn 2006; 35:1807–26.
[11] Usami T, Ge HB, Kasai A. Overall buckling prevention condition of buckling-restrained braces as a structural control damper. In: 14th world conference on earthquake engineering. 2008.
[12] Tsai KC, Hsiao BC, Wang KJ, Weng YT, Lin ML, Lin KC, Chen CH, Lai JW, Lin SL. Pseudo-dynamic tests of a full scale CFT/BRB frame—Part I: Specimen design, experiment and analysis. Earthq Eng Struct Dyn 2008;37:1081–98.
[13] Palazzo G, López-Almansa F, Cahís X, Crisafulli F. A low-tech dissipative buckling restrained brace. Design, analysis, production and testing. Eng Struct 2009;31:2152–61.
[14] Ju YK, Kim MH, Kim J, Kim SD. Component tests of buckling-restrained braces with unconstrained length. Eng Struct 2009;31:507–16.
[15] Celik OC, Bruneau M. Seismic behavior of bidirectional-resistant ductile end diaphragms with buckling restrained braces in straight steel bridges. Eng Struct 2009;31:380–93.
[16] AISC (American Institute of Steel Construction), Seismic provisions for structural steel buildings, Chicago, IL, 2005.
[17] Chen SY. Seismic tests and finite element analyses of buckling-restrained braces with a replaceable core plate. Thesis advisor: Chou CC. National Chiao Tung University, Hsinchu, Taiwan; 2008 [in Chinese].
[18] Chou CC, Chen SY. Subassemblage tests and finite element analyses of sandwiched buckling-restrained braces with a replaceable core. In: 6th international conference for behavior of steel structures in seismic area (STESSA). 2009.
[19] AISC (American Institute of Steel Construction). Manual of steel construction load and resistance factor design. Chicago, IL; 2005.
[20] ABAQUS. Standard user's manual version 6.3. Pawtucket, RI: Hibbitt, Karlsson & Sorensen, Inc.; 2003.
[21] Chou CC, Wu CC. Performance evaluation of steel reduced flange plate moment connections. Earthq Eng Struct Dyn 2007;36(14):2083–97.
[22] Wu CC. Seismic behavior of steel reduced flange moment connections. Thesis advisor: Chou CC. National Chiao Tung University, Hsinchu, Taiwan; 2005 [in Chinese].
[23] Chou CC, Chen JH, Chen YC, Tsai KC. Evaluating performance of post-tensioned steel connections with strands and reduced flange plates. Earthq Eng Struct Dyn 2006;35(9):1167–85.